Journal of Sound and Vibration (2002) **256**(1), 81–102
doi:10.1006/jsvi.2001.4201, available online at http://www.idealibrary.com on IDEAL®

DYNAMIC BEHAVIOUR OF A CRACKED SOLDERED JOINT

P. DINEVA

Institute of Mechanics, Bulgarian Academy of Sciences, Acad. G. Bonchev Street, bl. 4, 1113 *Sofia, Bulgaria*

D. GROSS

Institute of Mechanics, Darmstadt University of Technology, 64289 *Darmstadt, Germany*

AND

T. RANGELOV

Institute of Mathematics and Informatics, Bulgarian Academy of Sciences, 1113 *Sofia, Bulgaria*

(*Received* 4 *April* 2001, *and in final form* 2 *January* 2002)

The two-dimensional "in-plane" time-harmonic elastodynamic problem for a multi-layered cracked soldered joint system is studied. This problem is solved by using a hybrid of both displacement and hyper-singular traction boundary integral equation method. The proposed method directly accounts for the effect of the outer boundary of a finite multi-layered body and the interaction between the internal and interface cracks. The open fracture model is used to present the interface crack. Numerical results are shown and discussed to reveal the effect of the existence and sizes of cracks, the crack interaction, the debonding effect, the influence of the wave frequency and the type of the material combination on the crack-tip fracture parameters and the displacement scattered far field.

1. INTRODUCTION

Soldered joints are the base components of all electronic devices. Electronic industry products are considered as engineering systems for which the main functional characteristic is not only the mechanical load-carrying capacity but also the control of the electric charge transport driven by the applied electric loads. The mechanical stress and deformation during fabrication and service strongly influence the electronic transport characteristics. The existence of stress and strain fields in the electronic materials leads to the nucleation and the growth of defects. In his paper, Freund [1] defines a number of important specific research problems in the area of mechanics of electronic materials. He underlines the importance of the problem of an interfacial fracture in complex multi-layered electronic systems. Freund also mentioned that one of the major goals of the mechanics of electronic materials is to study the behaviour of cracks, holes and other defects with a view towards controlling them.

The main goal of this work is to formulate and to solve a two-dimensional (2-D) "in-plane" time-harmonic elastodynamic problem for wave propagation in a multi-layered soldered joint system: printed circuit board (PCB), thin base Cu layer with internal and interface cracks in it, and a soldered joint.

0022-460X/02/$35.00

This problem is solved by a hybrid use of both the displacement and hyper-singular traction boundary integral equations (BIE) with a parabolic type of discretization far from the crack tips and with a special parabolic quarter point (QP) and traction singular quarter point boundary elements (SQP-BE) near the crack tips. The proposed method accounts directly for the interaction of the waves diffracted at the crack tips of both cracks with those reflected from the boundary of the body and transmitted to the material interface, where a discontinuity of the material properties exists.

Two aspects are described:

- 2-D ultrasonic wave scattering by internal and interface cracks in a soldered joint. The evaluation of the wave–crack interaction and the scattered wave field is of practical importance for the ultrasonic non-destructive evaluation of the cracked state of the soldered joints. This directly concerns the monitoring of the electronic industry products.
- The assessment of the 2-D dynamic stress fields near cracks in the real soldered joint geometry and physics, in an evaluation of two fracture parameters: crack opening displacements (COD) and stress intensity factors (SIF). This information is important since the non-uniform stress and strain distribution is responsible for the microstructure changes in the soldered joint materials.

The literature review below considers two aspects: the dynamic behaviour of a finite multi-layered body with cracks in it (one or multiple interface/internal cracks) and the specific aspects of the numerical solution of these problems by BIEM.

The evaluation of the dynamic stress concentration field and the ultrasonic wave scattering field in a damaged soldered joint was studied in reference [2].

The anti-plane dynamic response of interface-cracked three-layered plates with isotropic/anisotropic layers is solved by the finite element method (FEM) in reference [3]. The results describe the interaction between the delamination and the transverse cracks in finite plates. A wave–crack and a crack–crack interaction in multi-layered plates are investigated in references [4–6]. The interface crack problems of a multi-layered anisotropic medium under a state of generalized plane deformation are considered in reference [7]. A new BIE formulation is proposed in reference [8] for a plane elastic body containing an arbitrary number of cracks and holes. Although this work relates to static cases, the same approach can be applied to the time-harmonic case.

As the boundary integral equation method (BIEM) will be used in the present work for the solution of the 2-D elastodynamic problem, the specific problems of the method will be discussed.

The direct application of the BIEM to crack problems leads to a degeneration if the two crack surfaces are considered co-planar, as is shown in references [9–11]. By imposing symmetrical boundary conditions and hence modelling only one crack surface, it is possible to overcome this difficulty for symmetrical crack geometry. For non-symmetrical crack problems, one of the following methods has to be applied: the Green function method [12], displacement discontinuity method [13], multi-domain method [14], body force method [12], non-hyper-singular traction BIE derived in references [15, 16], dual boundary element method proposed in references [17, 18], where the displacement BIE on one of the crack surfaces and the hyper-singular traction BIE on the other was applied. In reference [19], this last method is referred to as the natural boundary equation method (BEM) or canonical BIE, whilst in reference [20], it is referred to as a combination of displacement BIE and integrodifferential traction BIE and in reference [21], it is defined as a hybrid BIEM. Numerical treatment and regularization of 2-D hyper-singular BIE is given also in references [22, 23].

In the present work, the dual BEM is used for a solution of the non-symmetric problems of wave scattering by cracks in a soldered joint. The authors' papers [2] and [24] consider the similar problems for a cracked soldered joint system. While the results in reference [2] concern the evaluation of the stress concentration field in a soldered joint damaged by microcracks, in reference [24], the 2-D elastodynamic scattering problem is solved for the same soldered joint system but with a line macrocrack in one of the layers. The aim in the current work is to present a solution for the 2-D wave propagation problem in the same mechanical system where there is not only one internal crack but interface cracks also. Moreover, the crack interaction is accounted for when evaluating scattered wave and stress concentration fields.

The rest of the paper is organized as follows. The definition of the boundary-value problem is given in section 2. The hybrid usage of the displacement and the hyper-singular traction BIE for the solution of the formulated problem is considered in section 3. Section 4 focuses on the numerical solution procedure and its specific problems. Some results concerning the investigation of the accuracy and the convergence of the proposed numerical scheme are discussed in section 5. In section 6, details of a parametric study are described, which reveal the sensitivity of the scattered displacement wave field and near-tip fracture parameters to the various input data. Concluding remarks are given in section 7.

2. DESCRIPTION OF THE MODEL AND FORMULATION OF THE BOUNDARY-VALUE PROBLEM

2.1. OBJECT OF INVESTIGATION

A finite multi-layered body Ω containing an internal crack in one of the layers and an interface crack on the boundary between two layers is considered (see Figure 1). Let $\Omega = \Omega_1 \cup \Omega_2 \cup \Omega_3$, $\Gamma_\Omega = \partial\Omega$. The domain Ω_1 is the printed circuit board (PCB) with a boundary in the (x, y) plane $\Gamma_{\Omega_1} = LL_1H_1H$. The domain Ω_2 is the thin base layer with a boundary in the (x, y) plane $\Gamma_{\Omega_2} = HH_1Q_1Q$. There is a line crack MN in this layer with a surface $S_{MN\,cr} = S^+_{MN\,cr} \cup S^-_{MN\,cr}$. The region Ω_3 is the soldered joint with a boundary in the (x, y) plane $\Gamma_{\Omega_3} = BDCOA$. There is an interface crack EF on the boundary between the thin base layer and the soldered joint with a surface $S_{EF\,cr} = S^+_{EF\,cr} \cup S^-_{EF\,cr}$. The boundaries $S^+_{EF\,cr}$, $S^-_{EF\,cr}$, $S^+_{MN\,cr}$ and $S^-_{MN\,cr}$ are the upper and the lower crack surfaces respectively. The

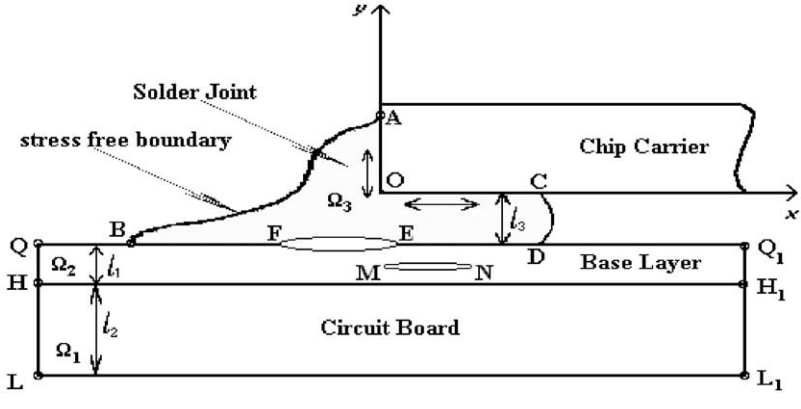

Figure 1. Solder joint geometry (2-D).

two crack surfaces are formed by the same set of points and all differences between them are due to the opposite normal directions. The corresponding material constants in the mth layer are the density ρ_m, Lame constants λ_m, μ_m and Poisson coefficient v_m. The material is linear elastic and isotropic and a plane strain state is assumed.

2.2. INCIDENT WAVE MOTION

Two problems due to incident time-harmonic load are studied:

Problem 1: *Excitation through prescribed displacements.* As the incident wave by the L-wave generator impinges on the multi-layered system (see Figure 1) scattered waves are generated. The receiver amplifier observes this scattered wave field. This loading case is described by an incident time-harmonic longitudinal L wave of the form $\tilde{u}_i(x, y, \omega, t) = u_{i0}(x, y, \omega) \exp(-\mathrm{i}\omega t)$ on LL_1, where $u_{i0}(x, y, \omega)$ is the wave amplitude, t the time and ω the frequency.

Problem 2: *Excitation through prescribed traction.* The dynamic stress field near the cracks in the soldered joint system due to the dynamic traction on the points $(x, y) \in LL_1$: $p_i(x, y, \omega, t) = p_{i0}(x, y) \exp(-i\omega t)$ on LL_1, where $p_{i0}(x, y)$ is the dynamic load amplitude.

2.3. THE GOVERNING EQUATIONS AND BOUNDARY CONDITIONS

The field equations in the time-harmonic case are given by

$$\sigma_{ij,j} + \rho_m \omega^2 u_i = 0 \tag{1}$$

in Ω_m, $m = 1, 2, 3$ and $\sigma_{ij} = C_{ijkl} u_{k,l}$, where $C_{ijkl} = \lambda \delta_{ij}\delta_{kl} + \mu(\delta_{ik}\delta_{jl} + \delta_{il}\delta_{jk})$, δ_{ij} is the Kronecker symbol.

The displacements u_i and stresses σ_{ij} satisfy the boundary conditions:

$$\begin{gathered}
\sigma^1_{ij} n_j|_{HH_1} = \sigma^2_{ij} n_j|_{HH_1}, \qquad u^1_i|_{HH_1} = u^2_i|_{HH_1}, \\
\sigma^2_{ij} n_j|_{DE \cup FB} = \sigma^3_{ij} n_j|_{DE \cup FB}, \qquad u^2_i|_{DE \cup FB} = u^3_i|_{DE \cup FB}, \\
\sigma_{ij} n_j = 0 \quad \text{for} \quad (x, y) \in AB \cup BQ \cup Q_1 D \cup DC \cup QL \cup L_1 Q_1, \\
u_i = 0 \quad \text{for} \quad (x, y) \in OA \cup OC, \\
\sigma_{ij} n_j|_{S^+_{cr}} = 0, \quad S^+_{cr} = S^+_{MN\,cr} \cup S^+_{EF\,cr}
\end{gathered} \tag{2}$$

and

$$u_i = u_{i0} \quad \text{for } (x, y) \in LL_1 \quad \text{(Problem 1)} \tag{3}$$

or

$$p_i = p_{i0} \quad \text{for } (x, y) \in LL_1 \quad \text{(Problem 2)}, \tag{4}$$

where $\sigma^l_{ij} = \sigma_{ij}|_{\Omega_l}$, $u^l_i = u_i|_{\Omega_l}$, $l = 1,2,3$ and n_j are the components of the exterior normal vector.

Rigid boundary conditions on the boundaries OA and OC will represent a damaged solder, softer than the chip carrier's material. The tractions p_i at the point $r = (x, y)$ on

a surface element are given by $p_i(r) = \sigma_{ij}(r)n_j(r) = P'_{ik}(n_r, \partial_r)u_k(r)$, where

$$P'_{ik}(n_r, \partial_r) = \lambda\, n_i(r)\,\partial_k + \mu n_k(r)\partial_i + \mu\delta_{ik}n_l(r)\partial_l, \quad \partial_l = \frac{\partial}{\partial r_l}. \tag{5}$$

The solution of the boundary-value problem is a vector-valued function $u_i(r, \omega) \in C^2(\Omega) \cap C^1(\Gamma_\Omega)$, such that $p_i(r, \omega) \in C^1(\Omega) \cap C(\Gamma_\Omega)$, which satisfy equation (1) and the boundary conditions (2), (3) for the Problem 1 and (2), (4) for the Problem 2. Here, $C^k(\Re)$ is the set of k times continuously differentiable functions in the domain $\Re$ (see reference [25]). Moreover, the behaviour near the crack tips ∂S_{cr}^+ of the displacement $u_i(r, \omega)$ is as $O(\sqrt{r})$ and of the traction $p_i(r, \omega)$ is as $O(1/\sqrt{r})$ (see reference [26]). Since the two boundary-value Problems 1 and 2 differ only by the boundary conditions on LL_1, the solution methods will be described simultaneously. The two problems will be separated when the numerical results are discussed.

The boundary-value problem is linear and the displacement $u_i(x, y, \omega)$ is in the form $u_i(x, y, \omega) = u_i^0(x, y, \omega) + u_i^c(x, y, \omega)$ and the traction $p_i(x, y, \omega)$ is in the form $p_i(x, y, \omega) = p_i^0(x, y, \omega) + p_i^c(x, y, \omega)$. Here the superscript 0 indicates the fields in the crack-free soldered joint in the presence of a prescribed external load, while c denotes the quantities in the cracked soldered joint under the loading conditions:

$$\begin{gathered} p_i^c = -\,p_i^0 \quad \text{on} \quad S_{cr}^+ = S_{MN\,cr}^+ \cup S_{FE\,cr}^+, \\ p_i^c = 0 \quad \text{on } \Gamma_p; \quad u_i^c = 0 \quad \text{on } \Gamma_u \quad \text{where } \Gamma_p \cap \Gamma_u = \Gamma_B;\ \Gamma_p \cap \Gamma_u \varnothing\ . \end{gathered} \tag{6}$$

3. BIE FORMULATION OF THE PROBLEM

The crack-free case is studied by the usage of the conventional displacement BIE. In the cracked case, a hybrid method of both a displacement and hyper-singular traction BIE is used. Here, (a) the displacement BIE describes the wave motion in the layers, where there is no internal crack or there is only interface-crack, i.e., between the PCB layer (Ω_1) and the soldered joint layer (Ω_3), while (b) the hyper-singular traction BIE describes the wave motion in the thin base layer (Ω_2), within an internal crack. The displacement BIE is applied on one of the interface-crack surfaces EF where the displacements are $u_{iFE\,cr}^{(3)}$ and the hyper-singular traction BIE is applied on the other surface EF, where the displacements are $u_{iEF\,cr}^{(2)}$ and $\Delta u_i^{EF} = u_{iFEcr}^{(3)} - u_{iFE\,cr}^{(2)}$ is the crack opening displacement on EF. The internal crack MN with its crack opening displacements $\Delta u_i^{MN} = u_i^{(2)}|_{S_{MN\,cr}^+} - u_i^{(2)}|_{S_{MN\,cr}^-}$ is a part of the boundary Γ_{Ω_2}, where traction BIE is applied.

3.1. CRACK-FREE STATE OF THE MULTI-LAYERED SOLDERED JOINT SYSTEM

The conventional displacement BIE:

$$c_{ij}\, u_j^0(r, \omega) = \int_{\Gamma_{\Omega_m}} U_{ij}^*(r, r_0, \omega) p_j^0(r_0, \omega)\, \mathrm{d}\Gamma - \int_{\Gamma_{\Omega_m}} P_{ij}^*(r, r_0, \omega)\, u_j^0(r_0, \omega) \mathrm{d}\Gamma \tag{7}$$

is used. Here, $m = 1, 2, 3$; c_{ij} are constants depending on the geometry at the collocation point r; r , r_0 denote the position vectors of the field and running points, respectively; U_{ij}^*, P_{ij}^* are the displacement and traction fundamental solutions of equation (1) corresponding to a time-harmonic load (see Appendix A).

Once the tractions p_i^0 on the boundaries S_{cr}^+ are determined, the second part of the solution (the cracked case) can be solved.

3.2. CRACKED STATE OF THE MULTI-LAYERED SOLDERED JOINT SYSTEM

For the layers Ω_1 and Ω_3 without an internal crack, the displacement BIE is used:

$$c_{ij}u_j^c(r,\omega) = \int_{\Gamma_{\Omega_m}} U_{ij}^*(r, r_0, \omega)p_j^c(r_0,\omega)\,\mathrm{d}\Gamma \; - \int_{\Gamma_{\Omega_m}} P_{ij}^*(r, r_0, \omega)u_j^c(r_0,\omega)\,\mathrm{d}\Gamma\,, \quad m = 1,3\,. \tag{8}$$

For the layer with an internal crack (the layer Ω_2), the system of hyper-singular traction BIE for the unknowns is used. Actually, these equations are traction boundary integrodifferential equations (BIDE) [20], since they contain tangential derivatives of the displacement. These derivatives are unbounded at the crack tips, due to the asymptotic behaviour of displacement as $\sqrt{r}$. The traction BIE is hyper-singular and some integrals do not converge even in the sense of Cauchy principal values (CPV). To circumvent this difficulty, the regularization technique of reference [27] is used. This regularization procedure uses partial integration to shift the derivatives of the traction fundamental solution to the derivatives of the unknown displacements and crack opening displacements. The traction BIEs for the domain Ω_2 after applying the regularization procedure from reference [27] read as

$$\begin{aligned}
&-p_l^0(\xi^+,\omega)\\
&\quad = \int_{\Gamma_{\Omega_2}} P'_{lk}U_{ks}^*(\eta,\xi^+,\omega)p_s^c(\eta,\omega)\,\mathrm{d}S_\eta\\
&\quad + C_{lpjr}n_p(\xi^+)\left\{C_{iskt}\left[\int_{S_{MNcr}^+} \Delta K_{rs}^i D_t U_{kj}^*(\eta-\xi^+,\omega)\,\mathrm{d}S_\eta + \int_{\Gamma_{\Omega_2}} K_{rs}^i D_t U_{kj}^*(\eta-\xi^+,\omega)\,\mathrm{d}S_\eta\right]\right.\\
&\quad \left. - \rho_2\,\omega^2\left[\int_{S_{MNcr}^+} \Delta u_i^{MN}(\eta,\omega)n_r(\eta)U_{ij}^*(\eta-\xi^+,\omega)\,\mathrm{d}S_\eta + \int_{\Gamma_{\Omega_2}} u_i^c n_r(\eta)U_{ij}^*(\eta-\xi^+,\omega)\,\mathrm{d}S_\eta\right]\right\}
\end{aligned} \tag{9}$$

$$\begin{aligned}
&p_l^c(\xi^*,\omega)\\
&\quad = \int_{\Gamma_{\Omega_2}} P'_{lk}U_{ks}^*(\eta,\xi^*,\omega)p_s^c(\eta,\omega)\,\mathrm{d}S_\eta\\
&\quad + C_{lpjr}n_p(\xi^*)\left\{C_{iskt}\left[\int_{S_{MNcr}^+} \Delta K_{rs}^i D_t U_{kj}^*(\eta-\xi^*,\omega)\,\mathrm{d}S_\eta + \int_{\Gamma_{\Omega_2}} K_{rs}^i D_t U_{kj}^*(\eta-\xi^*,\omega)\,\mathrm{d}S_\eta\right]\right.\\
&\quad \left. - \rho_2\,\omega^2\left[\int_{S_{MNcr}^+} \Delta u_i^{MN}(\eta,\omega)n_r(\eta)U_{ij}^*(\eta-\xi^*,\omega)\,\mathrm{d}S_\eta + \int_{\Gamma_{\Omega_2}} u_i^c n_r(\eta)U_{ij}^*(\eta-\xi^*,\omega)\,\mathrm{d}S_\eta\right]\right\}.
\end{aligned} \tag{10}$$

Here, $K_{rs}^i = [n_r(\eta)D_s - n_s(\eta)D_r]u_i(\eta,\omega)$, $\Delta K_{rs}^i = [n_r(\eta)D_s - n_s(\eta)D_r]\Delta u_i(\eta,\omega)$, $D_r = \partial/\partial\eta_r$ and the notations ξ^+, ξ^* for field points on S_{MNcr}^+ and Γ_{Ω_2}, respectively, are used.

The unknowns are the displacements and the tractions $u_i^0(r, \omega)$, $\mathrm{p}_i^0(r, \omega)$, $u_i^c(r, \omega)$, $p_i^c(r, \omega)$ on $\Gamma_{\Omega_1} \cup \Gamma_{\Omega_2} \cup \Gamma_{\Omega_3}$, displacements $u_{iFEcr}^{(3)}$ and $u_{iEFcr}^{(2)}$ on the interface crack S_{EFcr}^{+} and the crack opening displacement $\Delta u_i^{MN}(\eta, \omega)$ on S_{MNcr}^{+}. As far as equations (9) and (10) are BIDE, the functions K_{rs}^i and ΔK_{rs}^i have to be represented by the unknowns.

The set of BIE (7)–(10) together with the boundary conditions (2) and (3) for the Problem 1 or (2) and (4) for the Problem 2 describes the boundary-value problem for the dynamic behaviour of a finite cracked multi-layered soldered joint by displacement and hyper-singular traction BIE.

The solutions of both problems are vector-valued functions $u_i \in C^{1,\alpha}(\Gamma_\Omega)$ (correspondingly $p_i \in C^{0,\alpha}(\Gamma_\Omega)$), $0 < \alpha \leqslant 1$, i.e., its tangential derivatives on the boundary should be Hölder continuous (see reference [20]), where $C^{k,\alpha}(\Re)$ is the set of k times differentiable functions whose kth derivatives are Hölder continuous with a constant α. Under these conditions, the displacement BIE and the traction BIDE (9) and (10) are well-defined.

4. NUMERICAL SOLUTION PROCEDURE

A discretization of the boundaries is used: $\Gamma = \Gamma_{\Omega_1} \cup \Gamma_{\Omega_2} \cup \Gamma_{\Omega_3} \cup S_{cr}$. The components of the displacement and the traction on the sth BE are denoted by u_i^s, p_i^s. The following principles are used for the approximation of the displacement u_i, its tangential derivatives $u_{i,j}$ and the traction p_i:

(*Hö*) *Hölder continuity*: Functions $u_i \in C^{1,\alpha}(\Gamma)$, $\mathrm{u}_{i,j} \in C^{0,\alpha}(\Gamma)$, $p_i \in C^{0,\alpha}(\Gamma)$. These conditions have to be at least satisfied at the collocation points (see reference [20]).

(*Cr*) *Behaviour at the crack-tips*: The asymptotic behaviour of the displacement is as $u_i \sim O(\sqrt{r})$ and the asymptotic behaviour of the traction is as $p_i \sim O(1/\sqrt{r})$ (see reference [28]).

(*Irr*) *Irregular points*: A point at which the boundary is not smooth (correspondingly the normal vector does not exist), or the (Hö) conditions fail, is defined as an irregular point. The crack tip and the corners of a cracked body are particular examples of irregular points. Since the traction BIDE is well-defined only at the points where the interpolation functions are Hölder continuously differentiable and the boundary is smooth, the irregular points should not be used as collocation points.

Three nodes and three shape functions N_k determine the quadratic boundary element:

$$u_i^s(\xi) = \sum_1^3 u_i^{sk} N_k(\xi), \qquad p_i^s(\xi) = \sum_1^3 p_i^{sk} N_k(\xi). \tag{11}$$

Here, u_i^{sk} is the ith displacement component in the kth local node of the sth boundary element.

In order to satisfy the principle (Cr), two special crack-tip boundary elements are used: quarter-point boundary element (QP-BE) modelling the asymptotic behaviour of the displacement as $u_i \sim O(\sqrt{r})$ on the BE close to the crack tip and traction singular QP-BE (SQP-BE) modelling the asymptotic behaviour of traction $p_i \sim O(1/\sqrt{r})$ on the BE next to the crack tip.

Approximation functions (11) for u_i^s, p_i^s are continuous at the collocation points. The tangent derivatives of the displacements at the nodal points are expressed as derivatives of the approximated displacements. It is evident that the approximation of the tangent derivatives of the displacement does not satisfy (Hö) at the initial and at the final points on the boundary element.

In summary, the standard continuous quadratic approximation can be used only after overcoming the following disadvantages: the irregular points of a finite cracked body, i.e., crack tips and corners and the odd discretization nodes should not be used as collocation points. The traction BIDE is not well-defined at these points and this will lead to computational errors. In order to use the standard parabolic approximation avoiding the above-mentioned obstacles, it is necessary to choose an appropriate parabolic approximation for u_i, p_i, $u_{i,j}$ near the irregular point and near the odd collocation points so that the Hölder principle will be fulfilled. A numerical scheme for this aim is proposed below.

4.1. SHIFTED POINT NUMERICAL SCHEME

One possibility to use the standard parabolic approximation for u_i^s, p_i^s, $u_{i,j}^s$ is to use all even nodal points as collocation points, but instead of the odd nodal points to use points close to them. Consider the sth BE Γ^s with its nodal points z_1^s, z_2^s, z_3^s. The point $z_{11}^s \in (z_1^s, z_2^s)$ so that $z_{11}^s = z_1^s + \gamma(z_3^s - z_1^s)$, $\gamma > 0$ is used as a collocation point instead of the point z_1^s. Also the point $z_{11}^{s+1} \in (z_1^{s+1}, z_2^{s+1})$, where $z_{11}^{s+1} = z_1^{s+1} + \gamma(z_3^{s+1} - z_1^{s+1})$, $\gamma > 0$ is used as a collocation point instead of the point $z_3^s = z_1^{s+1}$. Note that now conditions (Hö) and (Irr) are fulfilled at all collocation points.

It is possible to express the unknowns u_i^s, p_i^s, $u_{i,j}^s$ at the collocation points, which are now internal points of the BE, by the unknowns at the geometrical nodes of the boundary element in order to form the global algebraic system for the unknowns at the boundary nodal points. If the unknowns at the nodes z_k^s are for example p_i^{sk}, and $\gamma > 0$ is small enough, $z_{11}^s = z_1^s + \gamma(z_3^s - z_1^s)$ is used as a collocation point. There is, on the other hand, an intrinsic co-ordinate $\xi_\gamma \in (-1, 1)$ corresponding to z_{11}^s and then $p_i^s(\xi_\gamma) = \sum_1^3 p_i^{sk} N_k(\xi_\gamma)$, where p_i^{sk} are the unknowns at the boundary element nodes. Using z_{11}^s as a collocation point, the equation $L_i(u_i, p_i) = p_i^s(\xi_\gamma)$ is obtained, where $L_i(u_i, p_i)$ is a linear expression of the unknowns at all nodal values. Or, having $L_i(u_i, p_i) = p_i^s(\xi_\gamma) = \sum_1^3 p_i^{sk} N_k(\xi_\gamma)$, then only the unknowns at the boundary nodes are used.

No problem arises when an internal crack in a finite body is considered. Then the crack tips are not used as collocation points and $\Delta u_i = 0$ and $p_i^c = -p_i^0$ at these points. A problem appears in the case of a crack, which lies or intersects the boundary. Here, a shift of the collocation point from the crack tip and from the other irregular points as corners is used.

So, using this numerical scheme of the shifted points all the necessary conditions for well-posed BIDE problem are satisfied. When the field point and the running point belong to the same BE, this scheme leads to singular integrals that are at least CPV integrals and are solved analytically. The solution of the integrals is obtained in two different cases with respect to the interval where the asymptotic expansion of the modified Bessel function $K_m(z)$ is applied (see Appendix A):

(i) The case when the asymptotic expansion for a small argument of the function $K_m(z)$ is applied to the whole BE.
(ii) The case when the asymptotic expansion for a small argument of the function $K_m(z)$ is applied only over a small range close to the collocation point and beyond this small range a numerical integration by the Gauss quadrature scheme is used.

It is important to note that the choice of case (i) or (ii) depends on the correct evaluation of the arguments of the functions $K_m(z)$. The limit for the asymptotic expansion for small

arguments is determined to be $|z_{lim\,it}| \leqslant 5$ (see reference [29]). Based on this, the relation between the minimal and the maximal BE lengths and the wavelength is evaluated.

4.2. SIF CALCULATION OF THE INTERFACE CRACK

The asymptotic solutions for the displacement u_i near the tip of a bi-material interface crack, were derived by Sun and Jih [30], based on the work of Rice and Sih [31]. K_{I}, K_{II} are not the classical modes I and II but they are reducible to the classical factors for a homogeneous material. Since the energy release rate is directly proportional toK_0^2, it is reasonable to choose $K_0 = |K| = \sqrt{K_{\mathrm{I}}^2 + K_{\mathrm{II}}^2}$ as a fracture parameter.

In order to represent K_{I}, K_{II} and $K_0 = \sqrt{K_{\mathrm{I}}^2 + K_{\mathrm{II}}^2}$ through COD of the interface crack Δu_i^{EF}, the asymptotic formulae

$$\Delta u_x = \sqrt{r} D_\varepsilon \{K_{\mathrm{I}}(\sin(\varepsilon \ln r) - 2\varepsilon \cos(\varepsilon \ln r)) + K_{\mathrm{II}}(\cos(\varepsilon \ln r) + 2\varepsilon \sin(\varepsilon \ln r))\},$$
$$\Delta u_y = \sqrt{r} D_\varepsilon \{K_{\mathrm{I}}(\cos(\varepsilon \ln r) + 2\varepsilon \sin(\varepsilon \ln r)) - K_{\mathrm{II}}(\sin(\varepsilon \ln r) - 2\varepsilon \cos(\varepsilon \ln r))\}$$

are used. Here

$$D_\varepsilon = \frac{1}{2\sqrt{2\pi} ch(\varepsilon\pi)} \left(\frac{k_2 + 1}{\mu_2} + \frac{k_3 + 1}{\mu_3} \right)$$

with $k_m = 3\text{–}4\nu_m, \quad m = 2, 3;$

$$\varepsilon = \frac{1}{2\pi} \ln \frac{1 + \beta}{1 - \beta} \quad \text{where} \quad \beta = \frac{1}{2} \frac{\mu_2(1 - 2\nu_3) - \mu_3(1 - 2\nu_2)}{\mu_2(1 - \nu_3) + \mu_3(1 - \nu_2)}.$$

From these expressions, the SIFs are obtained as

$$\begin{pmatrix} K_{\mathrm{I}} \\ K_{\mathrm{II}} \end{pmatrix} = \frac{1}{\sqrt{r} D_\varepsilon (1 + 4\varepsilon^2)} \begin{pmatrix} (\sin(\varepsilon \ln r) - 2\varepsilon \cos(\varepsilon \ln r)) & (\cos(\varepsilon \ln r) + 2\varepsilon \sin(\varepsilon \ln r)) \\ (\cos(\varepsilon \ln r) + 2\varepsilon \sin(\varepsilon \ln r)) & (-\sin(\varepsilon \ln r) + 2\varepsilon \cos(\varepsilon \ln r)) \end{pmatrix} \begin{pmatrix} \Delta u_x \\ \Delta u_y \end{pmatrix}$$

and

$$K_0 = \lim_{r \to 0} \frac{1}{\sqrt{r} D_\varepsilon \sqrt{1 + 4\varepsilon^2}} \sqrt{(\Delta \mathrm{u}_x^{EF})^2 + (\Delta u_y^{EF})^2}. \tag{12}$$

It is worth noting that the oscillatory terms are removed in equation (12) for the overall SIF K_0.

The validity of the open model chosen in this study might be seen from the asymptotic formulae (see reference [30]), for the stresses and the displacements of the interface crack. Note that:

(a) The overlapping zone of the CODs close to the crack tip and the zone of the oscillating stresses next to the crack tip are very small compared with l_{QP}—the length of the crack tip BE.
(b) The number of the points where the stress is zero are one or two in the interval close to the crack tip.
(c) The upper bound of the oscillating stresses is the stress with singularity of order $1/\sqrt{r}$. The maximum value of the integrals of stresses in the interval with oscillations is limited and small enough for small $|\varepsilon|$.

So, using BIEM for solution of the problem considered, the corresponding integrals in the oscillating zones are limited and smaller than the integrals of the stresses with a singularity as $O(1/\sqrt{r})$.

5. ACCURACY AND CONVERGENCE OF THE PROPOSED NUMERICAL SOLUTION PROCEDURE

The numerical results are obtained by a FORTRAN code and the aim of this section is to study the accuracy and convergence of the numerical procedure in a special test example. For this purpose, a rectangular plate without and with a centre crack is investigated in two cases:

Test example 1: Homogeneous plate under uniform time-harmonic tension (see Figure 2(a) and 2(b)). This example is solved by using the displacement BIE for a quarter of the geometry and the hyper-singular traction BIE for the whole geometry.

Test example 2: Bi-material plate under uniform time-harmonic tension (see Figure 3(a) and 3(b)). This test example is solved by using the displacement and the hyper-singular traction BIE for half of the geometry.

Note, that for $\varepsilon = 0$, i.e., in the homogeneous material case, both test examples have to give the same results. For the solution of the two test examples, the numerical scheme described in section 4 is used. Its accuracy and convergence is studied based on comparison with the results in reference [32], where the test example 1 is solved by displacement BIE for a quarter of the geometry.

The physical and geometrical properties of the central cracked plate are chosen as: density $\rho = 0{\cdot}5 \times 10^{-5}\text{kg/mm}^3$; Lame constant $\lambda = 0{\cdot}115385 \times 10^6\text{N/mm}^2$, the Poisson number $\nu = 0{\cdot}3$, shear modulus $\mu = 0{\cdot}76923 \times 10^5\text{N/mm}^2$, and the plate sizes 20 mm × 40 mm. The amplitude of the time-harmonic load is taken as $\sigma = 400\text{N/mm}^2$ and the crack size is 2a = 5 mm.

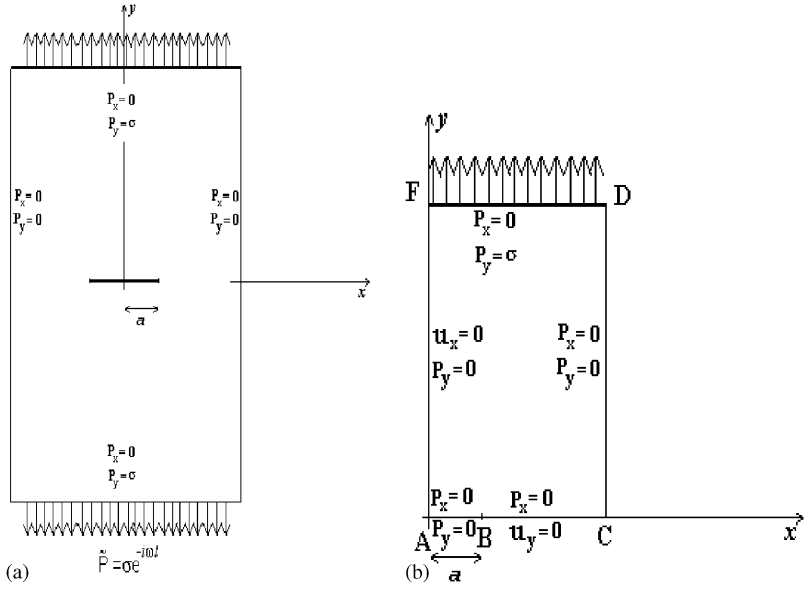

Figure 2. (a) A centrally cracked plate. (b) A quarter of the centre-cracked plate.

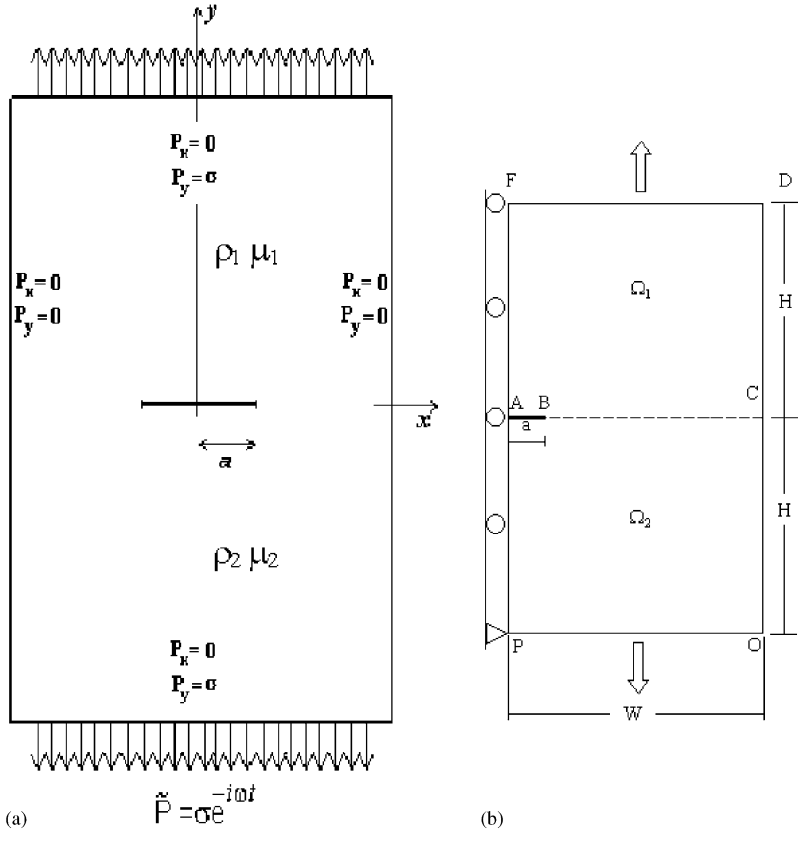

Figure 3. (a) A centre cracked bi-material plate. (b) A half of the centre-cracked bi-material plate.

TABLE 1

Physical constants

Number of range	Material	Density (kg/mm^3)	Lame constant (N/mm^2)	Poisson constant	Shear module (N/mm^2)	Wave shear velocity (mm/s)	Wave longitudinal velocity (mm/s)
Ω_1: Circuit board	Laminated insulation	$0{\cdot}1060 \times 10^{-5}$	$0{\cdot}9800 \times 10^4$	0·4000	$0{\cdot}245 \times 10^4$	$0{\cdot}15203 \times 10^7$	$0{\cdot}372322 \times 10^7$
Ω_2: Base layer	Cu	$0{\cdot}8960 \times 10^{-5}$	$0{\cdot}70724 \times 10^5$	0·2976	$0{\cdot}4810 \times 10^5$	$0{\cdot}231696 \times 10^7$	$0{\cdot}431624 \times 10^7$
Ω_3: Soldered joint	Pb	$0{\cdot}1140 \times 10^{-5}$	$0{\cdot}42007 \times 10^5$	0·4413	$0{\cdot}5590 \times 10^4$	$0{\cdot}700250 \times 10^6$	$0{\cdot}2160 \times 10^7$
	Sn	$0{\cdot}5750 \times 10^{-5}$	$0{\cdot}31637 \times 10^5$	0·2793	$0{\cdot}2500 \times 10^5$	$0{\cdot}2085 \times 10^7$	$0{\cdot}3768 \times 10^7$

The percentage error for SIF is defined as

$$Err = \frac{K_{\mathrm{I}}^{CD} - K_{\mathrm{I}}^{a}}{K_{\mathrm{I}}^{CD}} \%,$$

TABLE 2

Geometrical parameters

Boundary	Length (mm)
LL_1	4·0
HH_1	4·0
QQ_1	4·0
OA	1·0
CO	0·8
BQ	0·8
DB	2·0
Q_1B	1·2
DC	0·1
H_1Q_1	0·1
QH	0·1
L_1H_1	1·5
HL	1·5

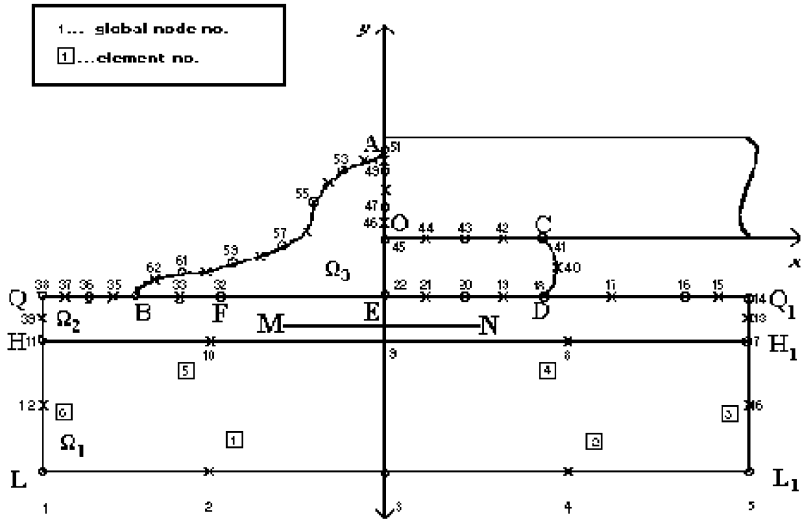

Figure 4. BE mesh.

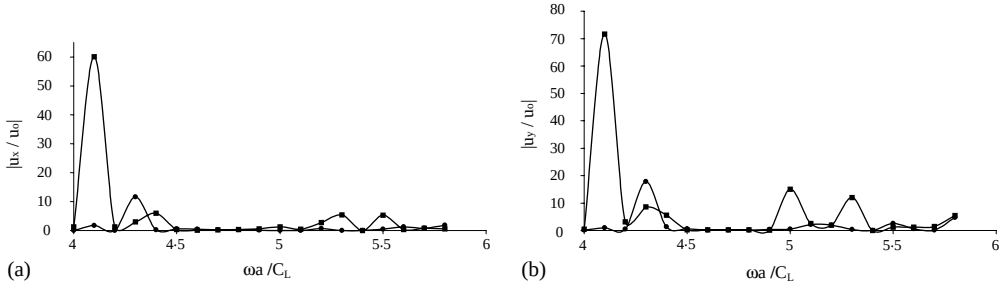

Figure 5. Displacement components of point 9 (see Figure 4) for Pb/Cu soldered joint versus frequency when there is an interface crack with length 0·4 mm: (a) $|u_x/u_0|$; (b) $|u_y/u_0|$; ●, uncracked case; ■, cracked case at $a = 0{\cdot}4$ mm.

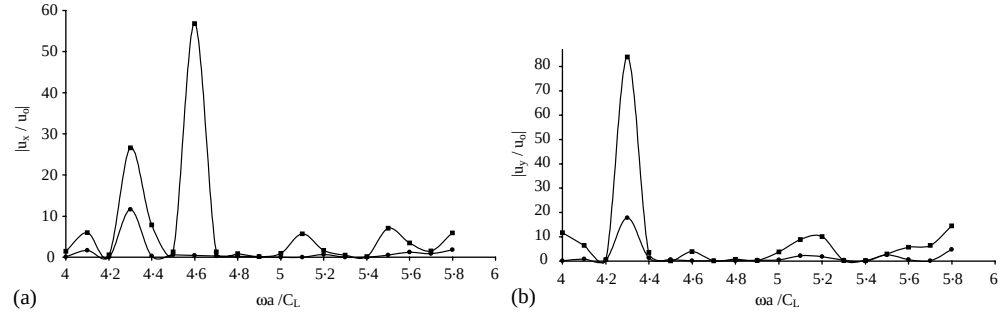

Figure 6. Displacement components of point 9 (see Figure 4) for Pb/Cu soldered joint versus frequency when there is an interface crack with length 0·8 mm: (a) $|u_x/u_0|$; (b) $|u_y/u_0|$; ●, uncracked case; ■, cracked case at $a = 0{\cdot}8$ mm.

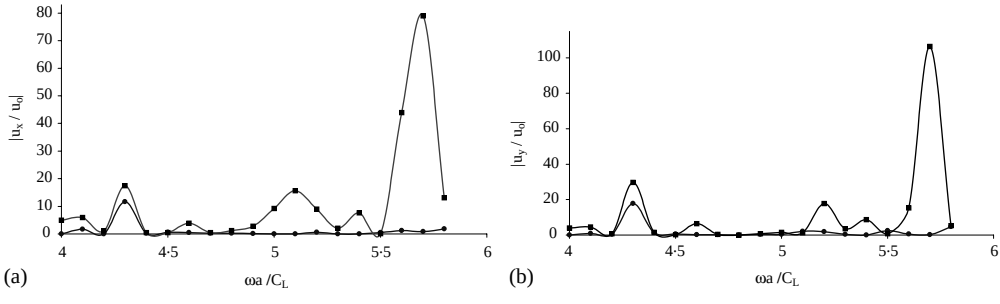

Figure 7. Displacement components of point 9 (see Figure 4) for Pb/Cu soldered joint versus frequency when there is an interface crack with length 1·6 mm: (a) $|u_x/u_0|$; (b) $|u_y/u_0|$; ●, uncracked case; ■, cracked case at $a = 1{\cdot}6$ mm.

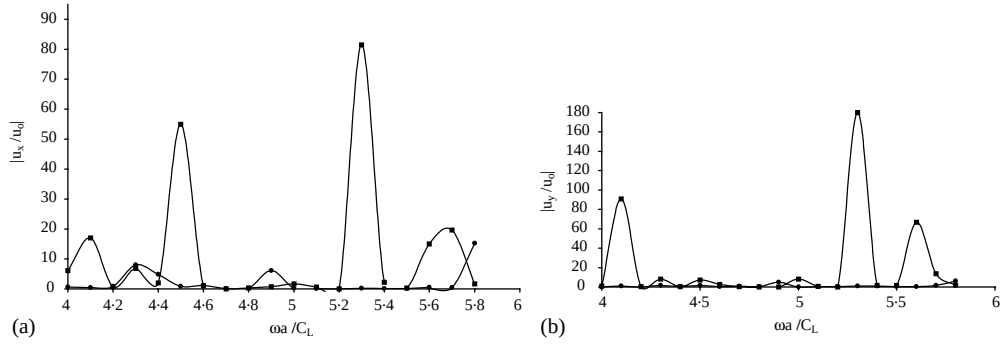

Figure 8. Displacement components of point 9 (see Figure 4) for Sn/Cu soldered joint versus frequency when there is an interface crack with length 0·4 mm: (a) $|u_x/u_0|$; (b) $|u_y/u_0|$; ●, uncracked case; ■, cracked case at $a = 0{\cdot}4$ mm.

where K_{I}^{CD} is the SIF from reference [32] and K_{I}^{a} is the SIF obtained in the present work. The numerical results obtained for both test examples show that the SIF calculation accuracy depends on the careful choice of the ratio l_{QP}/a and of the frequency. The minimal percentage error occurs close to 0·2 for l_{QP}/a and the maximal percentage error is no more than 4%.

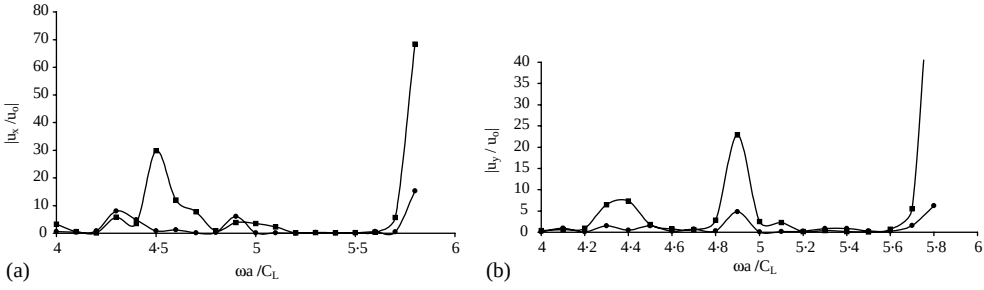

Figure 9. Displacement components of point 9 (see Figure 4) for Sn/Cu soldered joint versus frequency when there is an interface crack with length 0·8 mm: (a) $|u_x/u_0|$; (b) $|u_y/u_0|$; ●, uncracked case; ■, cracked case at $a = 0{\cdot}8$ mm.

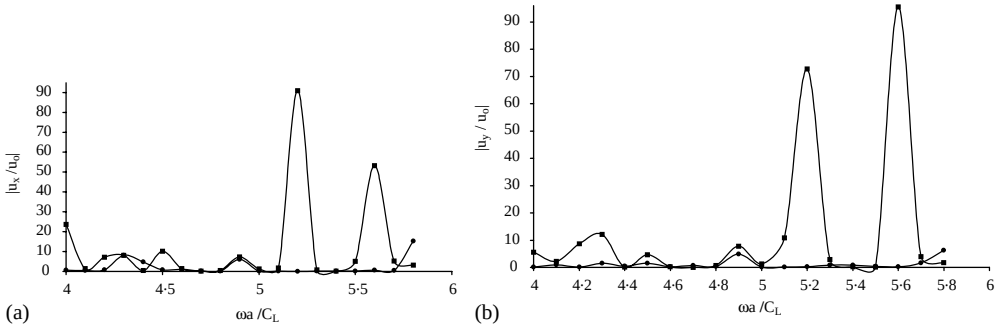

Figure 10. Displacement components of point 9 (see Figure 4) for Sn/Cu soldered joint versus frequency when there is an interface crack with length 1·6 mm: (a) $|u_x/u_0|$; (b) $|u_y/u_0|$; ●, uncracked case; ■, cracked case at $a = 1{\cdot}6$ mm.

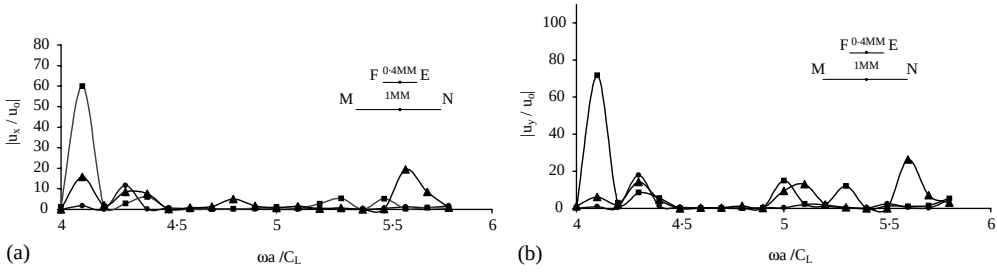

Figure 11. Displacement components of point 9 (see Figure 4) for Pb/Cu soldered joint versus frequency at existence of both cracks: (a) $|u_x/u_0|$; (b) $|u_y/u_0|$; ●, uncracked case; ■, interface-cracked case at $a = 0{\cdot}4$ mm; ▲, the case with both internal and interface cracks.

6. PARAMETRIC STUDY

The aim of this section is to reveal the sensitivity of the scattered wave field and near crack-tip fracture parameters with respect to:

- the type and frequency of the wave excitation;
- the type of material combination of the thin base layer/soldered joint;
- the existence, the location and the sizes of both cracks;

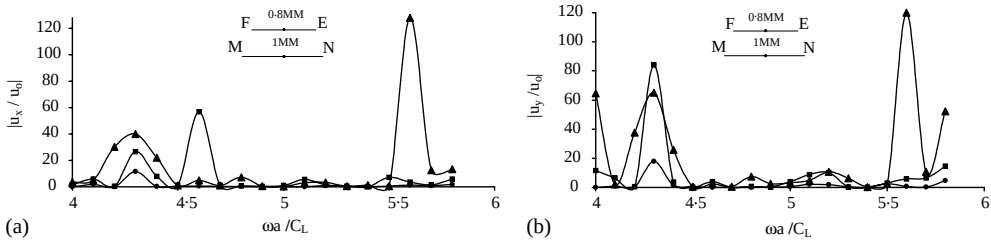

Figure 12. Displacement components of point 9 (see Figure 4) for Pb/Cu soldered joint versus frequency at existence of both cracks: (a) $|u_x/u_0|$; (b) $|u_y/u_0|$; ●, uncracked case; ■, interface-cracked case at $a = 0{\cdot}8$ mm; ▲, the case with both internal and interface cracks.

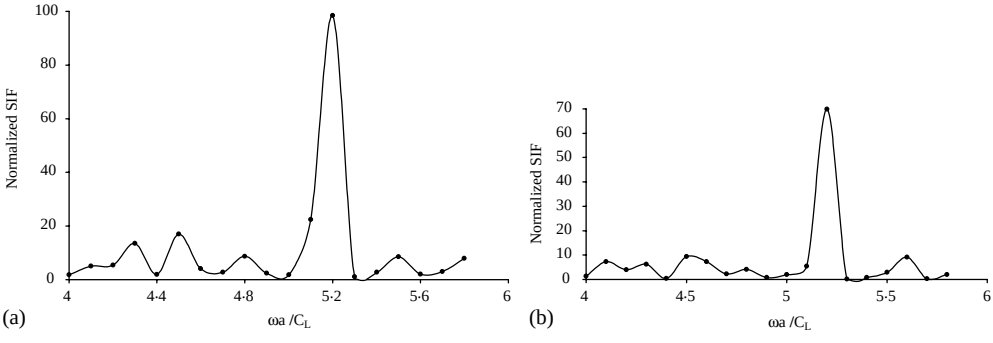

Figure 13. Normalized overall SIF for Pb/Cu soldered joint versus frequency when there is an interface crack with length 0·4 mm: (a) K_0^{left}; (b) K_0^{right}.

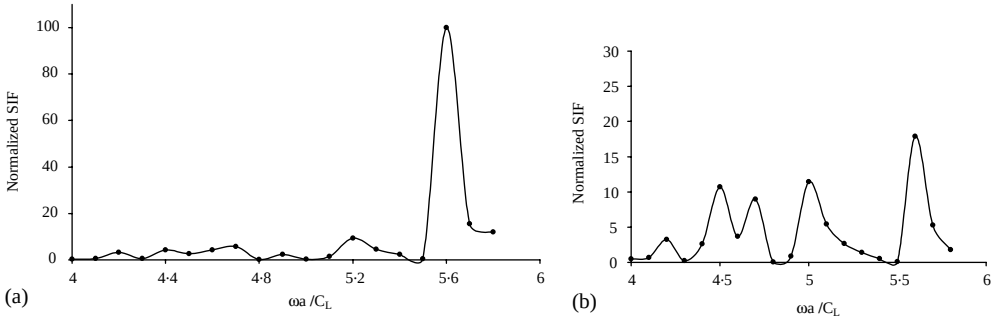

Figure 14. Normalized overall SIF for Sn/Cu soldered joint versus frequency when there is an interface crack with length 0·4 mm: (a) K_0^{left}; (b) K_0^{right}.

- the crack interaction between the internal crack inside the thin base layer and the interface crack on the boundary between the base layer and the soldered joint;
- the effect of debonding regions on the boundary between the base layer and the soldered joint, which is modelled as an interface crack with non-contacting faces.

The results obtained are interpreted from two different aspects:

- the evaluation of the scattered wave field and its practical importance to the application of ultrasonic non-destructive evaluation and monitoring of the cracked state of the soldered joints (solving Problem 1);

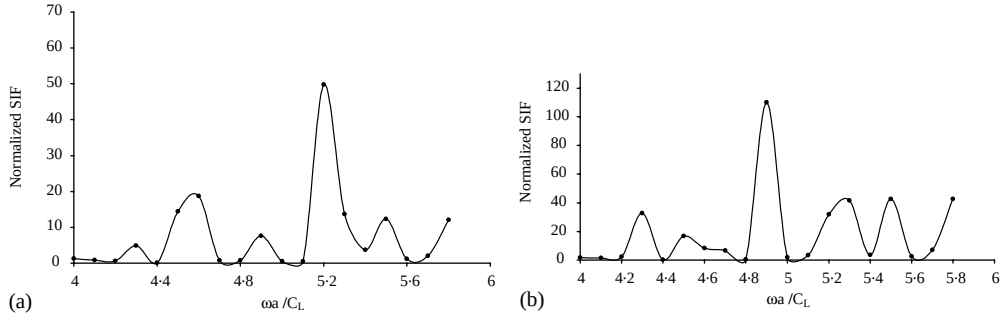

Figure 15. Normalized overall SIF for Pb/Cu soldered joint versus frequency when there is an interface crack with length 0·8 mm: (a) K_0^{left}; (b) K_0^{right}.

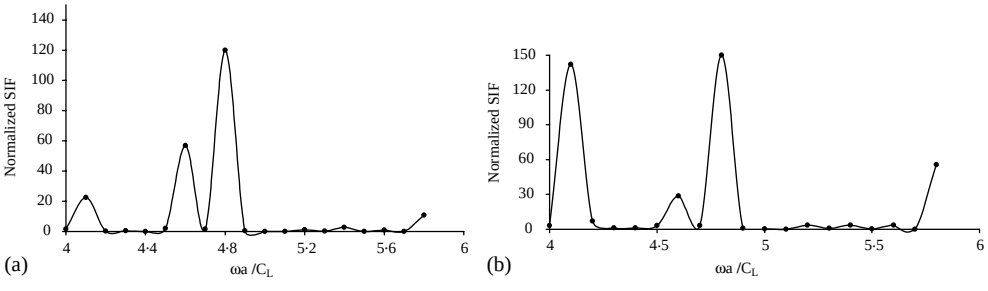

Figure 16. Normalized overall SIF for Sn/Cu soldered joint versus frequency when there is an interface crack with length 0·8 mm: (a) K_0^{left}; (b) K_0^{right}.

- the evaluation of fracture parameters in order to determine the fracture behaviour of soldered joints with real geometrical and mechanical properties (solving Problem 2).

The geometrical and mechanical characteristics of the multi-layered soldered joint system are given in Tables 1 and 2. The discretization mesh is presented in Figure 4. A FORTRAN code is used for a numerical solution of the problems. It is based on the numerical solution procedure described in section 4 and its accuracy and convergence is shown in section 5.

6.1. WAVE SCATTERING BY AN INTERNAL AND AN INTERFACE CRACK

In this case, the incident wave motion is given by a prescribed displacement and Problem 1 is solved.

6.1.1. *Scattered wave field on account of only an interface crack*

Figures 5–7 show the amplitude–frequency characteristics for both displacement components (u_x, u_y) of point 9 on the boundary H_1H (see Figure 4), when an interface crack exists with different lengths $a = 0{\cdot}4$, $0{\cdot}8$ and $1{\cdot}6$ mm, respectively, on the boundary between the thin base layer made of Cu and solder made of Pb. The amplitude of the incident L-wave is: $u_{x0} = 0$, $u_{y0} = u_0 = 0{\cdot}000001$ mm. The dimensionless parameter $\omega a/C_L$ is on the x-axis,

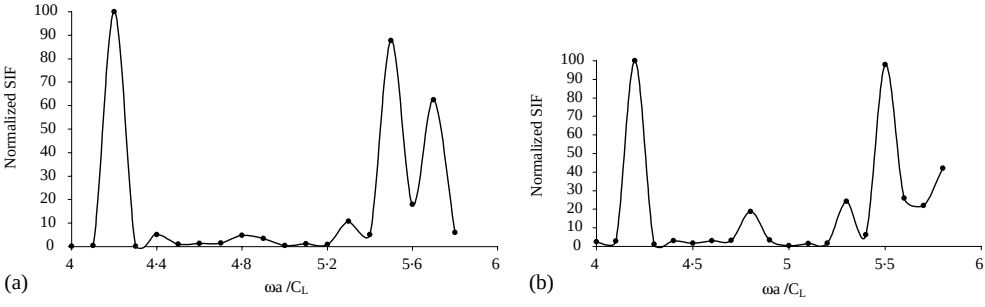

Figure 17. Normalized overall SIF for Pb/Cu soldered joint versus frequency when there is an interface crack with length 1·6 mm: (a) K_0^{left}; (b) K_0^{right}.

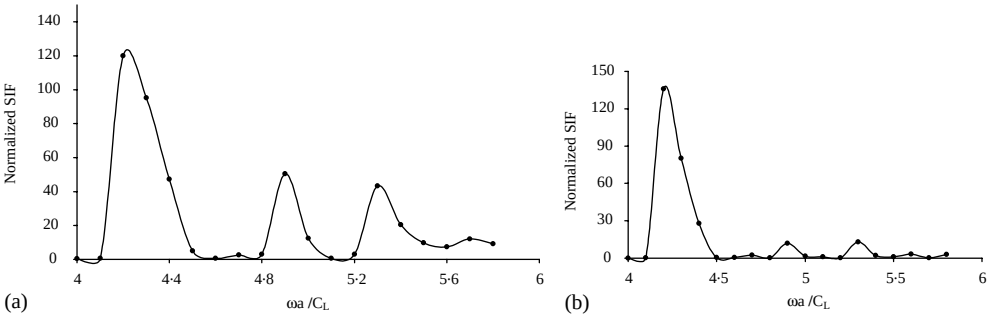

Figure 18. Normalized overall SIF for Sn/Cu soldered joint versus frequency when there is an interface crack with length 1·6 mm: (a) K_0^{left}; (b) K_0^{right}.

where a is the interface crack length and C_L is the longitudinal velocity in the base Cu layer. It is seen that when the debonding regions increase, the maximal displacement amplitude occurs at higher frequencies. The appearance of the resonance in the scattered fields suggests that it could be used in ultrasonic non-destructive evaluation to characterize large debonds in soldered joint systems. Therefore, it is important from a non-destructive testing point of view that a small amplitude of the incident pulse could excite a resonance.

The influence of the type of material combination on the character of the scattered field can be seen by comparing Figures 5–7 (solder/base layer: Pb/Cu) with Figures 8–10 (solder/base layer: Sn/Cu). There are resonance peaks in the displacement amplitudes for Sn/Cu case and small debond ranges in higher frequencies (see Figures 8 and 9), while there are no such peaks in Pb/Cu case (see Figures 5 and 6).

6.1.2. *Scattered wave field on account of both cracks*

An interface crack on the boundary between the thin base Cu layer and the soldered joint and an internal crack inside the base layer parallel to x-axis are now assumed. The length of the internal crack a_{MN} is 1 mm and it is centred at (0·0, − 0·16). The length of the interface crack EF is 0·4 or 0·8 mm and its centre is located at (0·0, − 0·1). The interaction between both the cracks is seen in Figures 11 and 12. The effect of the existence of the internal crack inside the base layer is stronger at higher frequencies and at longer interface cracks. At $\omega a/C_L = 4{\cdot}1$ (see Figure 11), the maximal amplitude strongly decreases in the case of both cracks.

6.2. NEAR-TIP FIELD PARAMETERS COD AND SIF

In this case, the incident wave motion is given by a prescribed traction and Problem 2 is solved.

6.2.1. *Fracture parameters in the presence of only an interface-crack*

Figures 13, 15 and 17 show, for the Pb/Cu material combination, the overall SIF—K_0^{right}, K_0^{left} calculated by equation (12) using the displacements at the right and left interface crack tips, respectively, in the case of a dynamic load $p_{x0} = 0$, $p_{y0} = \sigma \text{on} LL_1$. The overall SIF is normalized by $\sigma\sqrt{\pi a_{FE,\,cr}}$, where $\sigma = 1$ N/mm^2. Figures 14, 16 and 18 show, for the Sn/Cu material combination, the overall normalized SIF. All these figures present the frequency effect, the effect of existence of the interface crack, the effect of the material combination and the effect of the existence of the debonding on the boundary between the base layer and the soldered joint on the SIF values. With increasing debonding zone, the resonance peak of the SIF moves to the lower frequencies and this shift depends on the type of the material combination Pb/Cu or Sn/Cu.

6.2.2. *Fracture parameters in the case of both cracks*

Figures 19–21 show the normalized overall SIF at the crack tips of the interface crack in the presence of two cracks as described in section 6.1.2. The results show that the internal crack does not change the frequency character of the SIF curves and even the peak of the SIF at $\omega a/C_L = 5{\cdot}2$ (see Figure 19) decreases when there is an internal crack with a length of 1mm. The explanation of this effect can be given by the shadowing of the shorter interface crack ($a = 0{\cdot}4$ mm) by the longer internal one ($a_{MN\,cr} = 1$ mm). The situation is different when the interface crack is 0·8 and 1·6 mm respectively (see Figures 20 and 21). In these cases, the screen effect of the internal crack decreases. It is evident that the geometrical position of the two cracks is important when the crack interaction is evaluated. The illustration of this effect is presented in Figure 22, where the internal crack is located at two different places with respect to the interface crack $a = 0{\cdot}8$ mm:

- Case 1—centre of the internal crack is at (0·5, $-$ 0·16);
- Case 2—centre of the internal crack is at ($-$ 1·0, $-$ 0·12).

It can be seen that both different geometrical configurations of two cracks reflect on the value of the SIF obtained at the interface crack tips.

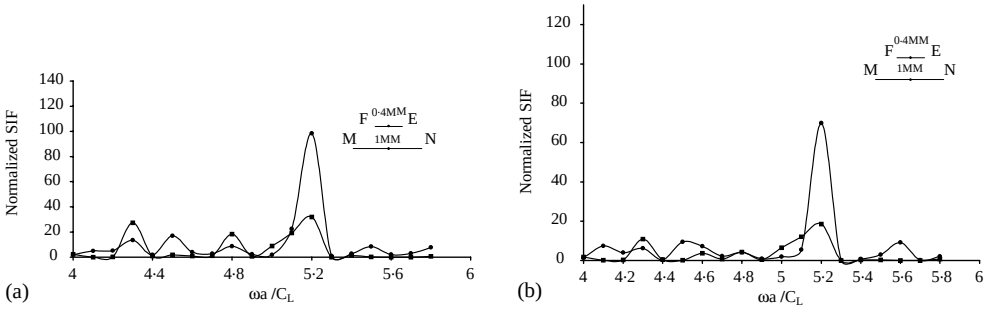

Figure 19. Normalized overall SIF for a Pb/Cu soldered joint versus frequency when there is an interface crack with length 0·4 mm and an internal crack inside the base layer: (a) K_0^{left}; (b) K_0^{right}; ●, interface-cracked case at $a = 0{\cdot}4$ mm; ■, the case with both internal and interface cracks.

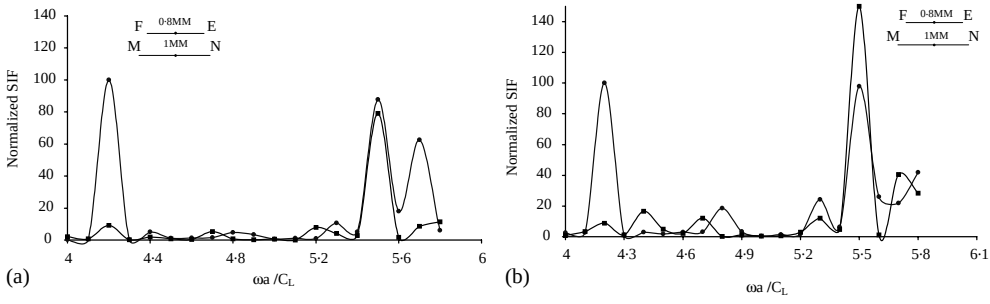

Figure 20. Normalized overall SIF for a Pb/Cu soldered joint versus frequency when there is an interface crack with length 0·8 mm and an internal crack inside the base layer: (a) K_0^{left}; (b) K_0^{right}; ●, interface-cracked case at $a = 0{\cdot}8$ mm; ■, the case with both internal and interface cracks.

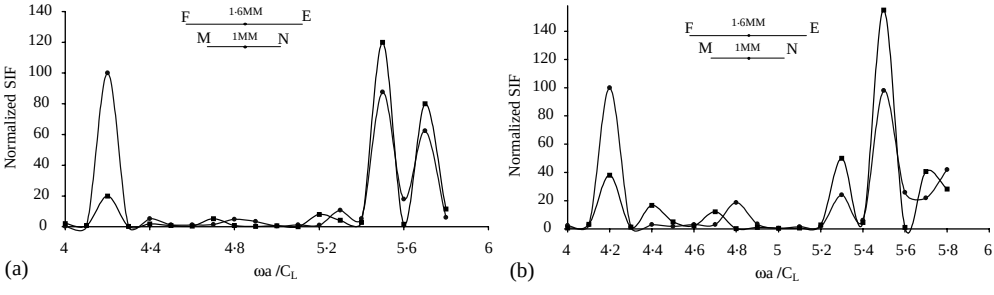

Figure 21. Normalized overall SIF for a Pb/Cu soldered joint versus frequency when there is an interface crack with length 1·6 mm and an internal crack inside the base layer: (a) K_0^{left}; (b) K_0^{right}; ●, interface-cracked case at $a = 1{\cdot}6$ mm; ■, the case with both internal and interface cracks.

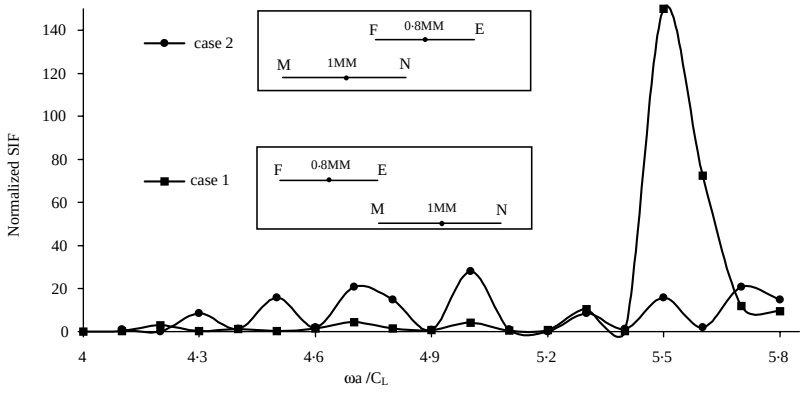

Figure 22. Normalized overall SIF K_0^{right} for a Pb/Cu soldered joint versus frequency when there is an interface crack with length 0·8 mm and an internal crack inside the base layer with co-ordinates of its centre: (a) case 1—(0·5, − 0·16); (b) case 2—(− 1·0, − 0·12).

7. CONCLUDING REMARKS

This paper presents a numerical solution of the 2-D elastodynamic problem for "in-plane" steady state wave propagation in a finite multi-layered body with different types

of cracks inside: either internal and/or interface. The crack interaction is accounted for by evaluation of both scattered wave fields far from the crack tips and local stress concentration fields near the crack tips. The problem is solved by dual BIEM with parabolic type of discretization and a shifted point numerical scheme.

The solution of the basic problem aims to study the mechanics of electronic materials–cracked soldered joint systems.

Numerical results obtained for a cracked soldered joint system (printed circuit board–thin base layer–soldered joint) show that:

- scattered wave far field and near-tip stress field are sensitive to the frequency of the incident wave, the interface-crack presence and the size and the material combination of the thin base layer and soldered joint;
- cracks influence each other under in-plane loading in a finite multi-layered body;
- the development of the debond zones reflects on the scattered wave and the stress picture. With the increasing debonding zone, the resonance peak of the SIF moves to the lower frequencies and this movement depends on the type of the material combination;
- the mutual configuration of cracks plays an important role in the evaluation of the soldered joint fracture state.

The present study, the developed numerical scheme and the created codes can be used for two main purposes: (a) monitoring the cracked and fracture state of the soldered joints; (b) understanding the processes that control the main function of the soldered joints to provide electrical and mechanical connection between different electronic chips.

ACKNOWLEDGMENT

The authors acknowledge the support of the Deutsche Forschungsgemeinschaft under Grant Number GR 596/29-1.

REFERENCES

1. L. B. FREUND 2000 *International Journal of Solids and Structures* **37**, 185–196. The mechanics of electronic materials.
2. P. DINEVA, D. GROSS and T. RANGELOV 1999 *Journal of Sound and Vibration* **223**, 213–230. Evaluation of scattered wave and stress concentration field in a damaged solder joint.
3. M. A. AWAL, T. KUNDU and S. P. JOSHI 1989 *Engineering Fracture Mechanics* **33**, 753–764. Dynamic behaviour of delamination and transverse cracks in fiber reinforced laminated composites.
4. T. KUNDU 1986 *Journal of Applied Mechanics* **53**, 579–586. Transient response of an interface-crack in a layered plate.
5. T. KUNDU 1988 *International Journal of Solids and Structures* **24**, 27–39. Dynamic interaction between two interface-cracks in a three layered plate.
6. T. KUNDU and T. HASSAN 1987 *International Journal of Fracture* **35**, 55–69. Numerical study of transient behaviour of an interface crack in a bi-material plate.
7. S. SHEN, Z. KUANG and S. HU 1999 *International Journal of Solids and Structures* **36**, 4251–4268. On interface crack in laminated anisotropic medium.
8. K. T. CHAU and Y. B. WANG 1999 *International Journal of Solids and Structures* **36**, 2041–2074. A new boundary integral formulation for plane elastic bodies containing cracks and holes.
9. T. A. CRUSE 1978 *Applied Mathematical Modelling* **2**, 287–293. Two-dimensional BIE fracture mechanics analysis.
10. D. E. BESKOS 1987 *Applied Mechanics Reviews* **40**, 1–23. BEM in dynamic analysis.
11. D. E. BESKOS 1988 *Applied Mechanics Reviews* **50**, 149–197. BEM in dynamic analysis II.

12. J. CHEN and H.-K. HONG 1999 *Applied Mechanics Reviews* **52**, 17–33. Review of dual boundary element methods with emphasis of hypersingular integrals and divergent series.
13. M. H. ALIABADI 1997 *Applied Mechanics Reviews* **50**, 83–96. Boundary element formulations in fracture mechanics.
14. M. H. ALIABADI 1997 *International Journal of Fracture* **86**, 91–125. A new generation of boundary element methods in fracture mechanics.
15. CH. ZHANG 1993 *Habilitationsschrift, TH-Darmstadt*. On Wave Propagation in Cracked Solids.
16. CH. ZHANG and D. GROSS 1998 *On Wave Propagation in Elastic Solids with Cracks*. Southampton: Computational Mechanics Publication.
17. A. PORTELA, M. H. ALIABADI and D. P. ROOKE 1992 *International Journal of Numerical Methods in Engineering* **33**, 1269–1287. Dual boundary element method: efficient implementation for cracked problems.
18. P. FEDELINSKI, M. H. ALIABADI and D. P. ROOKE 1996 *Computers and Structures* **59**, 1021–1031. The Laplace transform DBEM for mixed-mode dynamic analysis.
19. K. FENG 1983 *Proceedings of the International Congress of Mathematician, Warszawa*, 1439–1453. Finite element method and natural boundary reduction.
20. J. BALAS, J. SLADEK and V. SLADEK 1989 *Stress Analysis by BE*. New York: Elsevier.
21. F. CHIRINO and R. ABASCAL 1998 *International Journal of Numerical Methods in Engineering* **43**, 365–388. Dynamic and static analysis of cracks using the hypersingular formulation of the boundary element method.
22. A. SAEZ, R. GALLEGO and J. DOMINGUEZ 1995 *International Journal of Numerical Methods in Engineering* **38**, 1681–1701. Hypersingular quarter-point boundary elements for crack-problems.
23. R. GALLEGO and J. DOMINGUEZ 1997 *Fatigue and Fracture of Engineering Materials and Structures* **20**, 799–812. Solving transient dynamic crack problems by the hypersingular BEM.
24. P. DINEVA, D. GROSS and T. RANGELOV 1999 *Research in Nondestructive Evaluation* **11**, 117–135. Ultrasonic wave scattering by a line crack in a solder joint.
25. J. D. ACHENBACH 1973 *Wave Propagation in Elastic Solids*. New York: Elsevier.
26. V. KONDRATIEV 1967 *Proceedings of the Moscow Mathematical Society* **16**, 227–313. Boundary problems for elliptic equations in domain with conical and angular points.
27. V. SLADEK and J. SLADEK 1984 *Applied Mathematical Modelling* **8**, 2–10. Transient elastodynamic three-dimensional problems in cracked bodies.
28. G. E. BLANDFORD, A. R. INGRAFEA and J. A. LIGGET 1981 *International Journal of Numerical Methods in Engineering* **17**, 387–404. Two-dimensional stress intensity factor computations using the boundary element method.
29. J. DOMINGUEZ 1993 *Boundary Elements in Dynamics*. Southampton: Computational Mechanics Publication. Co-published with London: Elsevier Applied Science.
30. C. T. SUN and C. J. JIH 1987 *Engineering Fracture Mechanics* **28**, 13–20. On strain energy release rates for interfacial cracks in bi-material media.
31. J. R. RICE and G. C. SIH 1965 *Journal of Applied Mechanics* **32**, 418–423. Plane problems of cracks in dissimilar media.
32. F. CHIRINO and J. DOMINGUEZ 1989 *Engineering Fracture Mechanics* **34**, 1051–1061. Dynamic analysis of cracks using BEM.
33. H. BATEMAN and A. ERDELI 1953 *Higher Transcendental Functions*. New York: McGraw-Hill.

APPENDIX A

Function $U^*_{kj}(x, y, x_0, y_0, \omega)$ is the displacement at a point (x, y) in the kth direction due to the unit harmonic force with frequency ω applied in a point (x_0, y_0) in the jth direction, i.e., it is the solution of the equation

$$(\lambda + \mu) U^*_{lj,\,kl}(x, y, x_0, y_0, \omega) + \mu U^*_{kj,\,ll}(x, y, x_0, y_0, \omega) = -\delta_{kj}\,\delta(x - x_0, y - y_0),$$

where $\lambda = \lambda_n$ in Ω_n and $\mu = \mu_n$ in Ω_n, $n = 1, 2, 3$. The functions $P^*_{kj}(x, y, x_0, y_0, \omega)$ are the corresponding tractions. Let $r = \sqrt{(x^p - x^q)^2 + (y^p - y^q)^2}$, and $n = (n_x, n_y)$ be the unit

normal vector

$$r_{,x^q} = \frac{r_x}{r} = \frac{x^q - x^p}{r}, \quad r_{,y^q} = \frac{r_y}{r} = \frac{y^q - y^p}{r}, \quad \frac{\partial r}{\partial n} = r_{,x^q} n_x + r_{,y^q} n_y .$$

Note that (x^q, y^q) is a point running on the BE and (x^p, y^p) is the field point.

The functions $U^*_{kj}(x, y, x_0, y_0, \omega)$ and $P^*_{kj}(x, y, x_0, y_0, \omega)$ are represented by the modified Bessel functions of the second type $\mathrm{K}_m(z)$, where $\mathrm{K}_m(z) = -\frac{1}{2}\mathrm{i}\pi(i)^m \mathrm{H}^{(2)}_m(\mathrm{i}z)$. The functions $\mathrm{K}_m(z)$ are analytical functions for Im $z < 0$, and in the case considered $z = -(\mathrm{i}\omega/C_T)r$ or $z = -(\mathrm{i}\omega/C_L)r$. The following relations are fulfilled, see reference [33]:

$$\mathrm{K}_{m+1}(z) = \mathrm{K}_{m-1}(z) + \frac{2m}{z}\mathrm{K}_m(z); \quad \mathrm{K}_{m+1}(z) = -2\frac{\mathrm{d}}{\mathrm{d}z}\mathrm{K}_m(z) - \mathrm{K}_{m-1}(z).$$

Let $s = -\mathrm{i}\omega$ and $C_T^2 = \mu/\rho$, $C_L^2 = (\lambda + 2\mu)/\rho$. Then

$$\psi = \mathrm{K}_0\left(\frac{sr}{C_T}\right) + \frac{C_T}{sr}\left[\mathrm{K}_1\left(\frac{sr}{C_T}\right) - \frac{C_T}{C_L}\mathrm{K}_1\left(\frac{sr}{C_L}\right)\right], \qquad \chi = \mathrm{K}_2\left(\frac{sr}{C_T}\right) - \frac{C_T^2}{C_L^2}\mathrm{K}_2\left(\frac{sr}{C_L}\right).$$

The functions U^*_{kj}, P^*_{kj} and $U^*_{kj,l}$ have the form, where $k, j, l = x, y$:

$$U^*_{kj}(x^q - x^p, y^q - y^p, \omega) = \frac{1}{2\pi\mu}[\psi\,\delta_{kj} - \chi r_{,k}\, r_{,j}],$$

$$P^*_{kj}(x^q - x^p, y^q - y^p, \omega) = \frac{1}{2\pi}\left\{\left(\frac{\partial\psi}{\partial r} - \frac{\chi}{r}\right)\left(\delta_{kj}\frac{\partial r}{\partial n} + r_{,k}n_j\right) - 2\frac{\chi}{r}\left(r_{,j}\,n_k - 2r_{,k}r_{,j}\frac{\partial r}{\partial n}\right)\right\}$$

$$-\frac{1}{2\pi}\left\{2\frac{\partial\chi}{\partial r}r_{,k}\,r_{,j}\frac{\partial r}{\partial n} - \left(\frac{C_L^2}{C_T^2} - 2\right)\left(\frac{\partial\psi}{\partial r} - \frac{\partial\chi}{\partial r} - \frac{\chi}{r}\right)r_{,j}n_k\right\},$$

$$U^*_{kj,l}(x^q - x^p, y^q - y^p, \omega) = \frac{1}{2\pi\,\mu}\left\{\frac{\partial\psi}{\partial r}\,r_{,l}\delta_{kj} - \frac{\partial\chi}{\partial r}r_{,l}r_{,k}r_{,j} - \chi[r_{,kl}r_{,j} + r_{,k}r_{,jl}]\right\}.$$

To obtain the asymptotic representation of the above functions U^*_{kj}, P^*_{kj} and $U^*_{kj,l}$ for $r \to 0$, the following expressions are used for the modified Bessel functions (see reference [33]):

$$\mathrm{K}_0(z) \approx \ln\frac{2}{z}, \; \mathrm{K}_1(z) \approx \frac{1}{z} + \frac{1}{2}z\ln\frac{z}{2}, \; \mathrm{K}_2(z) \approx \frac{2}{z^2} \quad \text{for } z \to 0.$$

The asymptotic representations of the functions U^*_{kj}, P^*_{kj} and $U^*_{kj,l}$ for $r \to 0$ are

$$(U^*_{kj})^{as} \approx -\frac{1}{4\pi\,\mu}\left\{\left[\left(1 + \frac{C_T^2}{C_L^2}\right)\ln r + \ln\frac{\omega}{2C_T} + \frac{C_T^2}{C_L^2}\ln\frac{\omega}{2C_L}\right]\delta_{kj}\right.$$

$$\left.-\left(1 - \frac{C_T^2}{C_L^2}\right)r_{,k}r_{,j} + \mathrm{i}\,\frac{3\pi}{2}\left(1 + \frac{C_T^2}{C_L^2}\right)\right\},$$

$$(P^*_{kj})^{as} \approx -\frac{1}{2\pi r}\frac{C_T^2}{C_L^2}\left\{\left[\delta_{kj} - 2\left(1 - \frac{C_T^2}{C_L^2}\right)r_{,k}r_{,j}\right]\frac{\partial r}{\partial n} - [n_k r_{,j} - n_j r_{,k}]\right\},$$

$$(U^*_{kj,l})^{as} \approx -\frac{1}{4\pi\mu\, r}\left[\left(1 + \frac{C_T^2}{C_L^2}\right)r_{,l}\delta_{kj} - \left(1 - \frac{C_T^2}{C_L^2}\right)(r_{,j}\delta_{kl} + r_{,k}\delta_{jl}) + 2\left(1 - \frac{C_T^2}{C_L^2}\right)r_{,k}r_{,j}r_{,l}\right].$$